Hydrogen Sensing at Room Temperature Using Flame-synthesized Palladium-decorated Crumpled Reduced Graphene Oxide Nanocomposites

Mohammad Moein Mohammadi, Abhishek Kumar, Jun Liu†, Yang Liu, Thomas Thundat, Mark T. Swihart*

Department of Chemical and Biological Engineering, University at Buffalo, The State University of New York, Buffalo, NY 14260, USA

ABSTRACT: We present a unique three-dimensional palladium (Pd)-decorated crumpled reduced graphene oxide ball (Pd-CGB) nanocomposite for hydrogen (H_2) detection in air at room temperature. Pd-CGB nanocomposites were synthesized using a rapid continuous flame aerosol technique. Graphene oxide reduction and metal decoration occurred simultaneously in a high temperature reducing jet (HTRJ) process to produce Pd nanoparticles that were below 5 nm in average size and uniformly dispersed in the crumpled graphene structure. The sensors made from these nanocomposites were sensitive over a wide range of H_2 concentrations (0.0025-2%) with response value, response time, and recovery time of 14.8%, 73 s, and 126 s, respectively, at 2% H_2. Moreover, they were sensitive to H_2 in both dry and humid conditions. The sensors were stable and recoverable after 20 cycles at 2% H_2 with no degradation associated with volume expansion of Pd. Unlike other two-step methods for fabricating Pd-decorated graphene sensors, the HTRJ process enables a single-step formation of Pd- and other metal-decorated graphene nanocomposites with great potential for creating various gas sensors by simple drop-casting onto low-cost electrodes.

Hydrogen, a clean and sustainable energy carrier, has great potential for use as an alternative renewable fuel.[1, 2] However, broad consumer-level use of hydrogen as a fuel requires addressing key safety issues. Hydrogen is a colorless, odorless, and highly flammable gas with a lower explosive limit (LEL) of just 4% in air.[3] Thus, its leakage during production, transportation, and storage can have disastrous consequences.[4] In addition, hydrogen is used in many other areas, including the medical,[5] electronic,[2] metallurgical,[6] and aerospace industries.[7] For each of the mentioned applications, a specific H_2 concentration range is employed.[8, 9] Therefore, rapid, stable, low-cost, and accurate detection of H_2 for a wide range of concentrations, above and below the LEL, in air or in other gases, remains a crucial unmet need.[10]

Commercial chemo-resistive H_2 sensors are mainly based on metal oxides such as TiO_2, SnO_2, In_2O_3, and ZnO that usually work in a temperature range from 200 to 500°C.[11, 12] Maintaining high temperature increases power consumption and potentially introduces a source of ignition. In contrast, Pd selectively absorbs large volumetric quantities of H_2 at room temperature and forms palladium hydride (PdH_x), which results in an electrical resistivity change.[13] Pd-based hydrogen sensors have been widely investigated because of their safety, room temperature response, and low power consumption.[14] Such sensors can be divided into two main categories: Pd-film,[15] and Pd-nanostructure sensors including those based on Pd nanoparticles,[11] nanowires,[16] and nanocomposites.[17] Pd-film sensors generally exhibit slow response at low concentrations, and can be unreliable at high concentrations due to the volume expansion of PdH_x, leading to film deformation.[12] The volume expansion of PdH_x mainly depends on the H_2 concentration. PdH_x forms two phases: At relatively lower H_2 concentrations (H_2<1%), it forms an α-phase hydride (FCC); When the H_2 concentration reaches ~1%, a phase transition from α-phase to β-phase hydride (FCC) takes place.[18] The largest volume expansion happens at the phase transition concentration. Further increase in the H_2 concentration (>2%) does not increase the lattice constant noticeably because of H saturation in Pd.[19] Pd-nanostructure sensors can better tolerate these volume changes, but often exhibit low signal-to-noise responses and have very low conductance due to their discontinuous structures.[8, 20, 21]

Pd-nanocomposite sensors have shown great response and sensitivity for H_2 detection.[22] Pd is usually combined with or decorated on a conductive material to create a conduction path for chemoresistive H_2 sensors.[23] Among these materials, graphene is a promising candidate due to its unique features such as high surface area to volume ratio, structural flexibility, and high carrier mobility.[24] Although graphene itself is insensitive to H_2 gas, Pd-decorated graphene sensors benefit from a high electron mobility at room temperature and low electrical noise.[25, 26] There are various methods to make Pd-graphene nanocomposites with different morphologies such as Pd nanoparticles (NPs) on graphene sheets by chemical vapor deposition (CVD) - e-beam evaporation,[27] Pd NPs on graphene nanoribbons by CVD - laser lithography,[28] Pd-Pt NPs on reduced graphene oxide (rGO) by Hummers' - hydrothermal method,[29] and Pd-functionalized multi-layer graphene nanoribbon networks by mechanical exfoliation - e-beam evaporation.[30] However, most of these methods require two or more steps for graphene synthesis followed by Pd-decoration. Flame technology is widely used in industry for the large-scale production of various nanomaterials including titanium dioxide, fumed silica, and carbon black, as it offers a continuous, economical, and one-step synthesis approach.[31] However, despite the advantages of such techniques over other nanomaterials production processes, only a few studies have reported H_2 sensing applications of flame-made nanomaterials including Pd-loaded SnO_2 films,[32] Pt-loaded WO_3 films,[33] and AuPd-sensitized nanocrystalline SnO_2.[34] To the best of our knowledge, none have reported H_2 gas detection at room temperature using flame-made materials. On the other hand, recently, we have introduced a flame-

driven approach for the synthesis of metal-decorated three-dimensional (3D) reduced graphene oxide (rGO) nanocomposites.[35] Three-dimensional graphene nanostructures have been used for gas sensing applications because of their high accessible surface areas that improve the electron transfer between the materials and electrode surface.[36, 37] However, there are limited reports on the applications of these nanocomposites for H_2 sensing,[38] and to date, there is no report on room temperature Pd-3D graphene nanocomposite H_2 sensors. Development of these flame-made novel nanocomposites that benefit from a unique structure as well as ease of synthesis, can provide reliable sensors with low response and recovery times.

In this work, we present flame-synthesized Pd-CGB nanocomposites for room temperature H_2 detection in air. These nanocomposites are produced by a rapid, continuous high temperature reducing jet (HTRJ) process. A palladium nitrate precursor solution containing dispersed graphene oxide is injected into the reactor and Pd-CGB nanocomposites are produced in one step. We have characterized the Pd-CGBs by methods including electron microscopy, x-ray diffraction, and Raman spectroscopy and have evaluated sensors made from these nanocomposites for sensitivity over a wide range of H_2 concentrations (0.0025-2%) and for repeatability at a critical H_2 concentration (2%). Results show shorter response and recovery times for our sensor compared to previously reported Pd-graphene based hydrogen sensors in air at room temperature.

Experimental Section

Synthesis of Pd-CGB

Pd-CGBs were synthesized using the HTRJ process, as described in detail previously.[35] In this process, combustion products of a hydrogen-rich flame (H_2 (industrial grade, Airgas): 11 Standard Liters per Minute-SLM, O_2 (industrial grade, Airgas): 3.2 SLM, N_2 (Airgas): 5 SLM), passed through a converging-diverging nozzle. An aqueous dispersion of GO (0.5 mg/mL) (MSE supplies, Arizona) and palladium nitrate (Strem Chemical, Pd ≈40 %, 99.9 %-Pd) at a GO:Pd mass ratio of 2 (0.25 mg Pd/mL) was injected into the throat section of the nozzle using a syringe pump (Pharmacia P500) at 250 mL/h. The aqueous precursor was atomized by the hot high-velocity gas stream and the resulting droplets evaporated in the reducing environment of the reaction chamber containing excess H_2 at high temperature (≈550°C to 600°C). After the reaction zone, products were cooled and diluted immediately by mixing with 100 SLM nitrogen, and collected on a filter membrane (293 mm polyvinylidene fluoride (PVDF) filter membrane (Millipore-Sigma), 0.22 µm nominal pore size).

Material characterization

The size and morphology of Pd-CGBs were characterized using a JEOL JEM 2010 Transmission Electron Microscope (TEM) at 200 kV working voltage. 200-mesh copper TEM grids with a carbon support film were obtained from Ted Pella. A custom-built electrostatic sampler connected to the HTRJ process was used to collect nanomaterials directly from the aerosol product stream onto TEM grids for offline analysis. ImageJ software was used to determine the particle size distribution of Pd nanoparticles in Pd-CGB. High-resolution TEM (HRTEM) images were obtained using a FEI Tecnai G2 F30 at an accelerating voltage of 300 kV. High-angle annular dark-field scanning TEM (HAADF-STEM) images and STEM energy-dispersive X-ray spectroscopy (STEM-EDS) maps were collected using a JEOL JEM-ARM200F STEM at an accelerating voltage of 200 kV. A Cross-Beam® Focused Ion Beam-Scanning Electron Microscopy (FIB-SEM) Workstation (Carl Zeiss AURIGA) was used to observe the morphology of Pd-CGBs on the silicon interdigitated electrodes. The crystal structure of nanomaterials was determined by X-ray Diffraction (XRD) analysis (Bruker Ultima IV with Cu Kα X-ray source). Raman spectroscopy was employed to determine the structural properties of samples, using a Renishaw system with a 514 nm excitation laser focused through a 20× microscope objective. The Brunauer-Emmett-Teller (BET) surface area of Pd-CGB was measured by N_2 adsorption-desorption at 77 K (Micromeritics Tri-Star II). To determine the pore size distribution, Barrett-Joyner-Halenda (BJH) analysis was also employed. Before the measurement, the nanocomposite was dried in a vacuum oven at 80°C overnight followed by degassing at 150°C under vacuum for 2 h.

Hydrogen sensing measurements

H_2 sensors were prepared by drop-casting a 1 mg/mL Pd-CGB suspension produced by sonication in isopropyl alcohol (BDH 99.5%) onto a silicon interdigitated electrode (Newvision, Part No. INE Silicon FBA, line Width: 5µm, line space: 3µm). Then, the electrode was placed in a 100 cc micro-probe station (Nextron) connected to a multimeter (Keithley DMM6500) with controlled voltage. The electrical resistance was recorded over time using 2 probes on the electrodes. Two gas streams, dry air (Airgas, 3% H_2O) and H_2 in synthetic air (Airgas, 2% H_2), were controlled by mass flow controllers (MKS) to achieve specified gas flows and H_2 concentrations (0.0025-2%) entering the probe station. For all experiments reported here except for determining the limit of detection, the total gas flow was kept at 400 sccm at ambient temperature (~21°C). To achieve low H_2 concentrations (25 to 200 ppm), a total gas flow of 1000 sccm was used. Before the experiment, the sensor was kept under 2% H_2 (50 sccm) for 4 h followed by exposure to air (500 sccm) for 5 min. The sensitivity was defined by **Equation 1**:

$$S = \frac{R_s - R_0}{R_0} \times 100 \qquad (1)$$

Where R_0 and R_S are the sensor resistance before and after exposure to H_2 gas, respectively. The response and recovery times were defined as the time to reach 90% of the total measured resistance change following a step change in H_2 concentration. Step changes between 0% H_2 and fixed H_2 concentrations were made at 5 min intervals. A bubbler was added to the process before the micro-probe station to create humid conditions inside the chamber. Air with a relative humidity of ~95% (measured by a 2-channel compact USB temperature and humidity sensor from Thorlabs) was obtained for evaluating the sensor under humid environment.

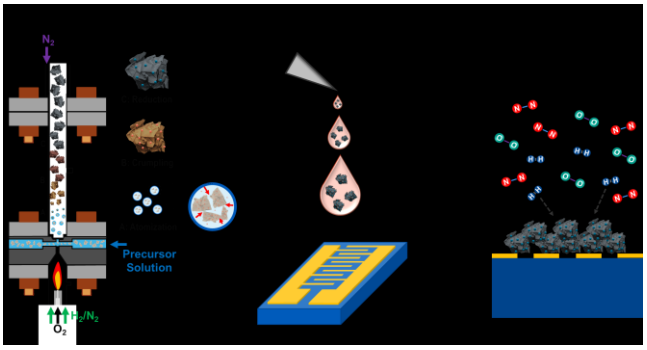

Figure 1. Schematic of Pd-CGB formation in the HTRJ process; sensor fabrication by drop-casting a Pd-CGB suspension produced by sonication in isopropyl alcohol onto an interdigitated electrode; and H_2 detection of the prepared electrode in air at room temperature. Part 1 of this figure was adapted from our previous study.[35]

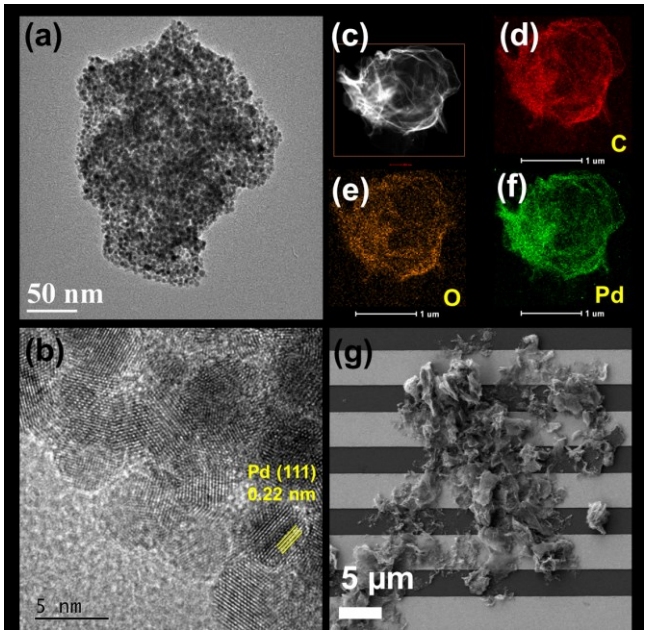

Figure 2. Representative Pd-CGB **a)** TEM image; **b)** HRTEM image; and **c-f)** HAADF-STEM image and corresponding elemental maps for C, O, and Pd; **g)** SEM image of the sensor prepared by simply drop-casting the Pd-CGB suspension on an interdigitated electrode.

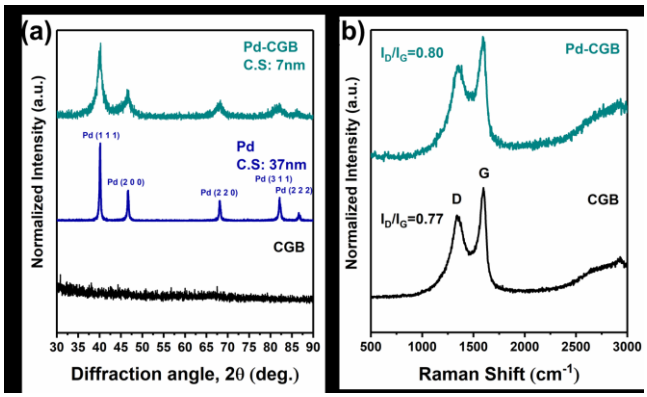

Figure 3. a) XRD patterns of CGB, unsupported Pd nanoparticles, and Pd-CGB; **b)** Raman spectra of CGB and Pd-CGB.

Results and Discussions

Figure 1 shows a schematic of (1) Pd-CGB production in the HTRJ process, (2) sensor fabrication, and (3) H_2 detection using the prepared sensor. Pd-CGB nanocomposites are produced in a reaction chamber with a H_2-rich reducing environment. Once the sensor is fabricated by simple drop-casting of a Pd-CGB suspension, H_2 detection is evaluated in the presence of O_2 and N_2 as shown in greater detail in **Figure S1**.

A representative TEM image of Pd-CGB is shown in **Figure 2a**. The crumpled ball is uniformly decorated with Pd nanoparticles. The minimal agglomeration suggests the gas phase nanocrystals grow from metal ions adsorbed on the surface of GO sheets. **Figure 2b** provides a representative HRTEM image of the nanocomposite. Pd nanoparticles are less than 5 nm in diameter and crystalline. Fringes have spacing of ~0.22 nm, consistent with the Pd (111) interplanar spacing. The calculated geometric mean diameter of nanoparticles based on the TEM image in **Figure S2** is 4.3 nm. **Figure 2c-f** displays an HAADF-STEM image with corresponding elemental maps for C, O, and Pd, respectively, from EDS analysis of a single Pd-CGB. Pd is well distributed over the CGB structure. As discussed thoroughly in previous work,[35] the oxygen-containing groups in GO are not reduced completely by the HTRJ process. Thus, the O elemental map reflects the oxygen groups still remaining in the CGB structure, along with any adsorbed oxygen-containing species. An SEM image of the deposited Pd-CGB on the interdigitated electrode is presented in **Figure 2g.** Smaller crumpled powders agglomerate and form larger micron-size structures providing continuous conduction pathways through the Pd-CGB network. As shown in **Figure S3**, the nanocomposite has a surface area of 73.14 m^2/g with BJH adsorption/desorption average pore width of 9.50/7.15 nm.

Figure 3a presents XRD patterns of CGB, unsupported Pd nanoparticles produced by the HTRJ process, and Pd-CGB nanocomposites. For comparison, the XRD pattern of Pd nanoparticles is also included. No crystalline structure is observed in this range for the CGB, although it usually has a broad peak between 20°–25° from the C (002) planes (not shown here). The XRD peaks for unsupported Pd nanoparticles are sharper than those of Pd-CGBs. The crystalline size of the two powders was estimated by the Debye−Scherrer equation based on the Pd (111) peak of the XRD patterns. The smaller crystalline size of Pd in Pd-CGB (7 nm), suggests that Pd nanoparticles in the Pd-CGB may grow directly on the GO surface. On the other hand, unsupported Pd nanoparticles (crystalline size: 37 nm), made by the gas-to-particle conversion mechanism, grow larger by aggregation and sintering processes. Pd-based XRD patterns match the FCC Pd reference pattern (PDF card no.: 00-005-0681) with no peaks corresponding to PdO. Raman spectra of CGB and Pd-CGB are shown in **Figure 3b**. The two major peaks at 1353 and 1597 cm^{-1} correspond to D- and G-bands. The G-band is assigned to sp^2-hybridized C atoms, and the D-band is attributed to defects in graphenic materials.[35] The intensity ratio (I_D/I_G) below 1 indicates a low concentration of defects in the CGB structure. However, with the addition of Pd, the ratio increases to 0.80 suggesting a higher degree of defects in the graphene structure when decorated with Pd nanoparticles.

The response of the Pd-CGB to a wide range of H_2 concentrations (0.01-2%) is presented in **Figure 4a**. The response and recovery times extracted from this figure are shown in **Figures S4** and **S5**. The sensitivity increases and the response time decreases with increasing H_2 concentration, because higher H_2 concentration in the vicinity of Pd nanoparticles enhances the diffusion of H atoms into the Pd lattice to form PdH_x. The sensor is almost recoverable at 5 min intervals without any noise in the resistance. **Figure 4b** displays the sensor response as a function of H_2 concentration for the Pd-CGB sensor. The response change is higher at low concentrations and plateaus at higher concentrations. Thus, as shown by others, it can be fit well by a logarithmic equation.[12, 29] At low H_2 concentrations, the sensor response is linearly proportional to the square root of the H_2 concentration (inset in **Figure 4b**). This relationship is explained by Sievert's law for H absorption.[39] Based on this phenomenon, H_2 molecules dissociate into H atoms at the surface of Pd to form a solid solution. At lower partial pressures of H_2, and when the dissolution equilibrium is reached, the partial pressure of H_2 surrounding the sensor and the H atom composition in the solid solution follow Sievert's law at constant temperature (**Equation 2**):[40, 41]

$$\text{Response} \propto x_H = \left(\frac{1}{K_s}\right) p_{H_2}^{0.5} \qquad (2)$$

Where K_s is the temperature-dependent Sievert constant; x_H is the number of hydrogen atoms per Pd atom, and approximately proportional to the response; and p_{H_2} is the H_2 gas concentration. Thus, the dissociative adsorption of H_2 into adsorbed H atoms on the surface of Pd surface and subsequent formation of PdH_x is the dominant mechanism for resistance change. After the hydride formation,

the graphene resistance increases due to electron transfer from PdH_x to graphene, reducing hole density in the p-type graphene.[12] Although graphene itself is insensitive to the physical adsorption of H_2, carbon atoms at the edges or defects of the CGB can form chemical bonds easily with dissociated hydrogen atoms. Thus, the fast response of the Pd-CGB can be attributed to the enhanced sensitivity and lower energy barrier of edges that allows fast charge transport between graphene and other absorbed materials.[42-44] As shown in **Figure 4c**, the sensor was exposed to ppm levels of H_2 (25 to 200 ppm) and gave a clear response to concentrations below 100 ppm, with an easily-detectable response of ~0.5% to 25 ppm H_2. The effect of humidity on the sensor is investigated in **Figure 4d**. For humid air, the sensor still responds to various H_2 concentrations (2, 1, 0.5, 0.25, 0.1 and 0.05%). For the humid condition, the baseline has been shifted to a higher resistance value compared with that of the dry condition. Moreover, the responses are closer to each other compared with those under dry conditions. Therefore, practical application of this sensor would require use in conjunction with a humidity sensor and humidity-dependent calibration, but it is expected to be usable over a broad range of relative humidity. **Figure 4e** exhibits the repeatability of Pd-CGB at the critical H_2 concentration of 2% for 20 cycles. As mentioned above, there is a

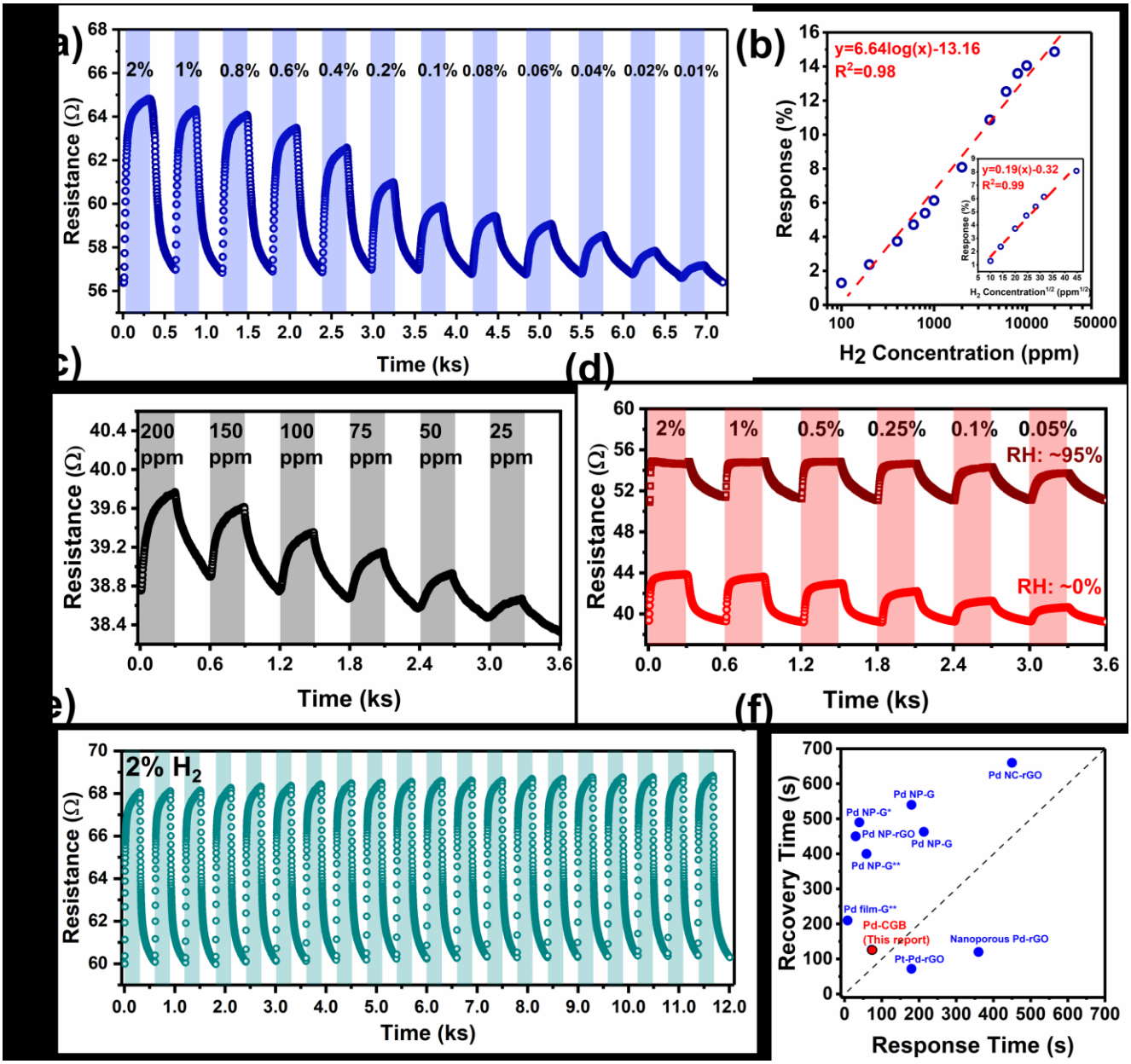

Figure 4. a) Sensitivity of Pd-CGB at different H_2 concentrations from 0.01% to 2%; **b)** response versus H_2 concentration with the fitted logarithmic equation for the data. The inset shows the response versus square root of concentration from 100 ppm to 2000 ppm and fitted by a linear equation; **c)** sensitivity of Pd-CGB sensor at ppm levels of H_2 from 25 ppm to 200 ppm; **d)** effect of humidity on the performance of the sensor at two relative humidity (RH) levels: RH ~ 0% and RH ~ 95%; **e)** repeatability test of Pd-CGB sensor at 2% H_2 for 20 cycles. (The darker regions in figures 4a,c,d,e are the 5 min intervals in which H_2 gas was flowing.); **f)** Comparison of the present work with other Pd-graphene based sensors for H_2 detection in air at room temperature: Pt-Pd-rGO,[45] Nanoporous Pd-rGO,[46] Pd film-G,[47] Pd NC-rGO,[48] Pd NP-rGO,[49] and Pd NP-G.[12, 27, 42, 50] (G: graphene, NC: nanocube). Note: in figure 4f: *defined as the time between 10% to 90% of the response; **defined as the time to reach (e^{-1}=36.8%) of the final value.

phase transition for palladium hydride at ~1%. The largest volume expansion takes place at the transition point and in the β-phase hydride region below 2%. Thus, testing the sensor at high concentrations as well as low concentrations is essential. The sensor was stable after 20 cycles with response value, response time and recovery time of 14.8%, 73 s, and 126 s, respectively. The performance of the current sensor compares favorably with other Pd-graphene sensors for H_2 detection in air at room temperature (**Table S1**). Overall, considering all the important factors defining a reliable sensor such as response value, response and recovery time, and wide sensing range, the Pd-CGB sensor provides a balance of features that may be superior to other reports in the literature. Some have reported a rapid response but a slow recovery, or a low LOD but a limited sensing range. Performance of the best sensors based on the lowest response/recovery times is summarized in **Figure 4f**. The Pd-CGB sensor is the closest point to the origin in a recovery versus response time graph. This implies that it not only exhibits rapid response, but also rapid recover, unlike some other sensors that exhibit fast response with a very slow recovery time. We also note that the response definitions, H_2 concentrations, and experimental setups differ for various prior reports, so direct comparisons must be made with caution.

Conclusion

We demonstrated the performance of sensors using three-dimensional Pd-decorated crumpled reduced graphene oxide nanocomposites for H_2 detection in air at room temperature. Pd-CGB nanocomposites were synthesized in a rapid, continuous aerosol flame-driven process. Palladium nanoparticles were <5 nm in average size and uniformly dispersed in the graphene structure, as demonstrated by electron microscopy and the corresponding elemental maps. Based on XRD patterns, crystalline non-oxide Pd-CGB nanocomposites were formed with smaller crystalline size compared with those of unsupported Pd nanoparticles produced by the same process. Raman spectra confirmed the graphitized structure of Pd-CGB even after metal decoration. The sensors made from these nanocomposites were sensitive over a wide range of H_2 concentrations (0.0025-2%) with short response and recovery times compared with other Pd-graphene based sensors reported in the literature. The response was logarithmic with respect to H_2 concentration over a wide range, but was better fit by Sievert's law at low concentrations. The LOD of the sensor was 25 ppm and the response, response time, and recovery time for 2% H_2 were 14.8%, 73 s, and 126 s, respectively. The sensor was sensitive to H_2 under humid conditions (relative humidity of ~95%). The presence of edges and defects in the crumpled graphene structure may provide enhanced sensitivity and faster charge transport. The sensor was stable after 20 cycles at 2% H_2 and did not show any degradation due to the cyclic volume expansion and contraction of Pd upon hydrogen uptake and release.

ASSOCIATED CONTENT

Supporting Information

Supporting information available: Schematic of the sensor testing setup, TEM image and the corresponding particle size distribution, BET and BJH analysis of Pd-CGB, response and recovery times at different H_2 concentrations, and a detailed table summarizing performance of reported Pd-graphene-based sensors at room temperature in air.

AUTHOR INFORMATION

Corresponding Author

Mark T. Swihart, Email: swihart@buffalo.edu

Present Addresses

†Current Affiliation: Department of Mechanical and Aerospace Engineering and RENEW Institute, University at Buffalo, The State University of New York

Author Contributions

The manuscript was written through contributions of all authors. All authors have given approval to the final version of the manuscript.

Notes

The authors declare no competing financial interests.

ACKNOWLEDGMENT

This work was supported in part by the National Science Foundation (CBET-1804996) and the New York State Center of Excellence in Materials Informatics.

REFERENCES

1. Nugroho, F. A. A.; Darmadi, I.; Cusinato, L.; Susarrey-Arce, A.; Schreuders, H.; Bannenberg, L. J.; da Silva Fanta, A. B.; Kadkhodazadeh, S.; Wagner, J. B.; Antosiewicz, T. J.; Hellman, A.; Zhdanov, V. P.; Dam, B.; Langhammer, C., Metal–polymer hybrid nanomaterials for plasmonic ultrafast hydrogen detection. *Nat. Mater.* **2019,** *18*, 489-495.

2. Wang, F.; Hu, K.; Liu, H.; Zhao, Q.; Wang, K.; Zhang, Y., Low temperature and fast response hydrogen gas sensor with Pd coated SnO_2 nanofiber rods. *Int. J. Hydrogen Energy* **2020**.

3. Liu, Q.; Yao, J.; Wu, Y.; Wang, Y.; Ding, G., Two operating modes of palladium film hydrogen sensor based on suspended micro hotplate. *Int. J. Hydrogen Energy* **2019,** *44*, 11259-11265.

4. Weber, M.; Kim, J. Y.; Lee, J. H.; Kim, J. H.; Iatsunskyi, I.; Coy, E.; Miele, P.; Bechelany, M.; Kim, S. S., Highly efficient hydrogen sensors based on Pd nanoparticles supported on boron nitride coated ZnO nanowires. *J. Mater. Chem. A* **2019,** *7*, 8107-8116.

5. Ge, L.; Yang, M.; Yang, N.-N.; Yin, X.-X.; Song, W.-G., Molecular hydrogen: a preventive and therapeutic medical gas for various diseases. *Oncotarget* **2017,** *8* (60), 102653-102673.

6. Ramachandran, R.; Menon, R. K., An overview of industrial uses of hydrogen. *Int. J. Hydrogen Energy* **1998,** *23* (7), 593-598.

7. Cecere, D.; Giacomazzi, E.; Ingenito, A., A review on hydrogen industrial aerospace applications. *Int. J. Hydrogen Energy* **2014,** *39* (20), 10731-10747.

8. Zheng, L.; Zheng, S.; Wei, H.; Du, L.; Zhu, Z.; Chen, J.; Yang, D., Palladium/Bismuth/Copper Hierarchical Nano-Architectures for Efficient Hydrogen Evolution and Stable Hydrogen Detection. *ACS Appl. Mater. Interfaces* **2019,** *11*, 6248-6256.

9. Kim, D. H.; Kim, S. J.; Shin, H.; Koo, W. T.; Jang, J. S.; Kang, J. Y.; Jeong, Y. J.; Kim, I. D., High-Resolution, Fast, and Shape-Conformable Hydrogen Sensor Platform: Polymer Nanofiber Yarn Coupled with Nanograined Pd@Pt. *ACS Nano* **2019,** *13*, 6071-6082.

10. Miliutina, E.; Guselnikova, O.; Chufistova, S.; Kolska, Z.; Elashnikov, R.; Burtsev, V.; Postnikov, P.; Svorcik, V.; Lyutakov, O., Fast and All-Optical Hydrogen Sensor Based on Gold-Coated Optical Fiber Functionalized with Metal-Organic Framework Layer. *ACS Sens.* **2019**, acssensors.9b01074.

11. Du, L.; Yuan, M.; Wei, H.; Xing, X.; Feng, D.; Liao, Y.; Chen, H.; Yang, D., Interconnected Pd Nanoparticles Supported on Zeolite-AFI for Hydrogen Detection under Ultralow Temperature. *ACS Appl. Mater. Interfaces* **2019,** *11*, 36847-36853.

12. Tang, X.; Haddad, P. A.; Mager, N.; Geng, X.; Reckinger, N.; Hermans, S.; Debliquy, M.; Raskin, J. P., Chemically deposited palladium nanoparticles on graphene for hydrogen sensor applications. *Sci. Rep.* **2019,** *9* (1), 3653.

13. Kumar, A.; Mohammadi, M. M.; Swihart, M. T., Synthesis, growth mechanisms, and applications of palladium-based nanowires and other one-dimensional nanostructures. *Nanoscale* **2019**, *11*, 19058-19085.

14. Cho, M.; Zhu, J.; Kim, H.; Kang, K.; Park, I., Half-Pipe Palladium Nanotube-Based Hydrogen Sensor Using a Suspended Nanofiber Scaffold. *ACS Appl. Mater. Interfaces* **2019,** *11*, 13343-13349.

15. Hu, Y.; Lei, J.; Wang, Z.; Yang, S.; Luo, X.; Zhang, G.; Chen, W.; Gu, H., Rapid response hydrogen sensor based on nanoporous Pd thin films. *Int. J. Hydrogen Energy* **2016,** *41*, 10986-10990.

16. Du, L.; Feng, D.; Xing, X.; Fu, Y.; Fonseca, L. F.; Yang, D., Palladium/cobalt nanowires with improved hydrogen sensing stability at ultra-low temperatures. *Nanoscale* **2019,** *11*, 21074-21080.

17. Peng, Y.; Zheng, L.; Zou, K.; Li, C., Enhancing performances of a resistivity-type hydrogen sensor based on Pd/SnO_2/RGO nanocomposites. *Nanotechnology* **2017,** *28* (21), 215501.

18. Favier, F.; Walter, E. C.; Zach, M. P.; Benter, T.; Penner, R. M., Hydrogen Sensors and Switches from Electrodeposited Palladium Mesowire Arrays. *Science* **2001,** *293* (5538), 2227.

19. Li, X.; Cao, T.; Zhang, X.; Sang, Y.; Yang, L.; Wang, T.; Li, Y.; Zhang, L.; Guo, L.; Fu, Y., Characterization and optimization of the H_2 sensing performance of Pd hollow shells. *Sens. Actuators, B* **2019,** *295*, 101-109.

20. Lee, J. S.; Seo, M. H.; Choi, K. W.; Yoo, J. Y.; Jo, M. S.; Yoon, J. B., Stress-engineered palladium nanowires for wide range (0.1%-3.9%) of H_2 detection with high durability. *Nanoscale* **2019,** *11*, 16317-16326.

21. Liu, Q.; Yao, J.; Wang, Y.; Sun, Y.; Ding, G., Temperature dependent response/recovery characteristics of Pd/Ni thin film based hydrogen sensor. *Sens. Actuators, B* **2019,** *290*, 544-550.

22. Sharma, B.; Kim, J. S., MEMS based highly sensitive dual FET gas sensor using graphene decorated Pd-Ag alloy nanoparticles for H_2 detection. *Sci. Rep.* **2018,** *8,* 5902.

23. Yokoyama, T.; Tanaka, T.; Shimokawa, Y.; Yamachi, R.; Saito, Y.; Uchida, K., Pd-Functionalized, Suspended Graphene Nanosheet for Fast, Low-Energy Multimolecular Sensors. *ACS Appl. Nano Mater.* **2018,** *1* (8), 3886-3894.

24. Hong, J.; Lee, S.; Seo, J.; Pyo, S.; Kim, J.; Lee, T., A highly sensitive hydrogen sensor with gas selectivity using a PMMA membrane-coated Pd nanoparticle/single-layer graphene hybrid. *ACS Appl. Mater. Interfaces* **2015,** *7*, 3554-3561.

25. Kumar, R.; Malik, S.; Mehta, B. R., Interface induced hydrogen sensing in Pd nanoparticle/graphene composite layers. *Sens. Actuators, B* **2015,** *209*, 919-926.

26. Zhu, J.; Cho, M.; Li, Y.; Cho, I.; Suh, J.-H.; Del Orbe, D.; Jeong, Y.; Ren, T.-L.; Park, I., Biomimetic Turbinate-like Artificial Nose for Hydrogen Detection Based on 3D Porous Laser-Induced Graphene. *ACS Appl. Mater. Interfaces* **2019,** *11*, 41.

27. Wu, W.; Liu, Z.; Jauregui, L. A.; Yu, Q.; Pillai, R.; Cao, H.; Bao, J.; Chen, Y. P.; Pei, S.-S., Wafer-scale synthesis of graphene by chemical vapor deposition and its application in hydrogen sensing. *Sens. Actuators, B* **2010,** *150* (1), 296-300.

28. Pak, Y.; Kim, S. M.; Jeong, H.; Kang, C. G.; Park, J. S.; Song, H.; Lee, R.; Myoung, N.; Lee, B. H.; Seo, S.; Kim, J. T.; Jung, G. Y., Palladium-decorated hydrogen-gas sensors using periodically aligned graphene nanoribbons. *ACS Appl. Mater. Interfaces* **2014,** *6* (15), 13293-8.

29. Peng, Y.; Ye, J.; Zheng, L.; Zou, K., The hydrogen sensing properties of Pt–Pd/reduced graphene oxide based sensor under different operating conditions. *RSC Adv.* **2016,** *6* (30), 24880-24888.

30. Johnson, J. L.; Behnam, A.; Pearton, S. J.; Ural, A., Hydrogen sensing using pd-functionalized multi-layer graphene nanoribbon networks. *Adv. Mater.* **2010,** *22* (43), 4877-80.

31. Mohammadi, M. M.; Gunturi, S. S.; Shao, S.; Konda, S.; Buchner, R. D.; Swihart, M. T., Flame-synthesized nickel-silver nanoparticle inks provide high conductivity without sintering. *Chem. Eng. J.* **2019,** *372*, 648-655.

32. Liewhiran, C.; Tamaekong, N.; Wisitsoraat, A.; Tuantranont, A.; Phanichphant, S., Ultra-sensitive H_2 sensors based on flame-spray-made Pd-loaded SnO_2 sensing films. *Sens. Actuators, B* **2013,** *176*, 893-905.

33. Samerjai, T.; Tamaekong, N.; Liewhiran, C.; Wisitsoraat, A.; Tuantranont, A.; Phanichphant, S., Selectivity towards H_2 gas by flame-made Pt-loaded WO_3 sensing films. *Sens. Actuators, B* **2011,** *157* (1), 290-297.

34. Krivetskiy, V.; Zamanskiy, K.; Beltyukov, A.; Asachenko, A.; Topchiy, M.; Nechaev, M.; Garshev, A.; Krotova, A.; Filatova, D.; Maslakov, K.; Rumyantseva, M.; Gaskov, A., Effect of AuPd Bimetal Sensitization on Gas Sensing Performance of Nanocrystalline SnO_2 Obtained by Single Step Flame Spray Pyrolysis. *Nanomaterials* **2019,** *9* (5).

35. Mohammadi, M. M.; Shao, S.; Srivatsa Gunturi, S.; Raghavan, A. R.; Alexander, N.; Liu, Y.; Stafford, C. M.; Buchner, R. D.; Swihart, M. T., A general approach to multicomponent metal-decorated crumpled reduced graphene oxide nanocomposites using a flame-based process. *Nanoscale* **2019,** *11* (41), 19571-19578.

36. Nazarian-Samani, M.; Kim, H.-K.; Park, S.-H.; Youn, H.-C.; Mhamane, D.; Lee, S.-W.; Kim, M.-S.; Jeong, J.-H.; Haghighat-Shishavan, S.; Roh, K.-C.; Kashani-Bozorg, S. F.; Kim, K.-B., Three-dimensional graphene-based spheres and crumpled balls: micro- and nano-structures, synthesis strategies, properties and applications. *RSC Adv.* **2016,** *6* (56), 50941-50967.

37. Xia, Y.; Li, R.; Chen, R. S.; Wang, J.; Xiang, L., 3D Architectured Graphene/Metal Oxide Hybrids for Gas Sensors: A Review. *Sensors* **2018,** *18* (5), 21.

38. Phan, D.-T.; Youn, J.-S.; Jeon, K.-J., High-sensitivity and fast-response hydrogen sensor for safety application using Pt nanoparticle-decorated 3D graphene. *Renewable Energy* **2019,** *144*, 167-171.

39. Ollagnier, A.; Fabre, A.; Thundat, T.; Finot, E., Activation process of reversible Pd thin film hydrogen sensors. *Sens. Actuators, B* **2013,** *186*, 258-262.

40. Yu, K.; Tian, X.; Wang, X.; Yang, F.; Qi, T.; Zuo, J., Enhanced accuracy of palladium-nickel alloy based hydrogen sensor by in situ temperature compensation. *Sens. Actuators, B* **2019,** *299*, 126989.

41. Ju, S.; Lee, J. M.; Jung, Y.; Lee, E.; Lee, W.; Kim, S.-J., Highly sensitive hydrogen gas sensors using single-walled carbon nanotubes grafted with Pd nanoparticles. *Sens. Actuators, B* **2010,** *146* (1), 122-128.

42. Yi, J.; Kim, S. H.; Lee, W. W.; Kwon, S. S.; Sung, W. N.; Park, W. I., Graphene meshes decorated with palladium nanoparticles for hydrogen detection. *J. Phys. D: Appl. Phys.* **2015,** *48* (47).

43. Yi, J.; Lee, D. H.; Lee, W. W.; Park, W. I., Direct Synthesis of Graphene Meshes and Semipermanent Electrical Doping. *J. Phys. Chem. Lett.* **2013,** *4* (13), 2099-2104.

44. Wang, X.; Li, X.; Zhang, L.; Yoon, Y.; Weber, P. K.; Wang, H.; Guo, J. Dai, H., N-Doping of Graphene Through Electrothermal Reactions with Ammonia. *Science* **2009,** *324* (5928), 768.

45. Phan, D.-T.; Uddin, A. S. M. I.; Chung, G.-S., A large detectable-range, high-response and fast-response resistivity hydrogen sensor based on Pt/Pd core–shell hybrid with graphene. *Sens. Actuators, B* **2015,** *220*, 962-967.

46. Phan, D.-T.; Chung, G.-S., A novel nanoporous Pd–graphene hybrid synthesized by a facile and rapid process for hydrogen detection. *Sens. Actuators, B* **2015,** *210*, 661-668.

47. Lim, J.; Hwang, S.; Yoon, H. S.; Lee, E.; Lee, W.; Jun, S. C., Asymmetric electron hole distribution in single-layer graphene for use in hydrogen gas detection. *Carbon* **2013,** *63*, 3-8.

48. Phan, D.-T.; Chung, G.-S., Effects of Pd nanocube size of Pd nanocube-graphene hybrid on hydrogen sensing properties. *Sens. Actuators, B* **2014,** *204*, 437-444.

49. Martínez-Orozco, R. D.; Antaño-López, R.; Rodríguez-González, V., Hydrogen-gas sensors based on graphene functionalized palladium nanoparticles: impedance response as a valuable sensor. *New J. Chem.* **2015,** *39* (10), 8044-8054.

50. Alfano, B.; Massera, E.; Polichetti, T.; Miglietta, M. L.; Di Francia, G., Effect of palladium nanoparticle functionalization on the hydrogen gas sensing of graphene based chemi-resistive devices. *Sens. Actuators, B* **2017,** *253*, 1163-1169.

For TOC use only